

www.acsami.org Forum Article

Alkyne Hydrogenation Catalysis across a Family of Ga/In Layered Zintl Phases

Kelsey L. Hodge and Joshua E. Goldberger*



Cite This: ACS Appl. Mater. Interfaces 2021, 13, 52152-52159



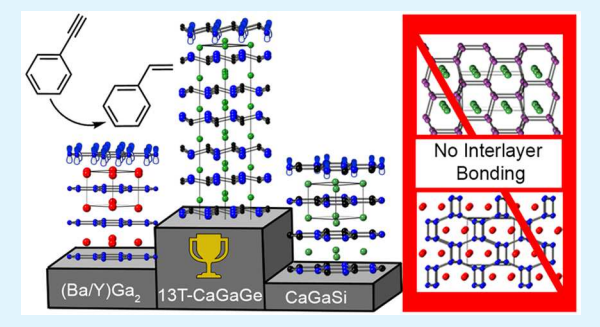
ACCESS

III Metrics & More



SI Supporting Information

ABSTRACT: Transition-metal-free Zintl–Klemm phases have received little attention as heterogeneous catalysis. Here, we show that a large family of structurally and electronically similar layered Zintl–Klemm phases built from honeycomb layers of group 13 triel (Tr) or group 14 tetrel (Tt) networks separated by electropositive cations (A) and having a stoichiometry of ATr₂ or ATrTt (A = Ca, Ba, Y, La, Eu; Tr = Ga, In; Tt = Si, Ge) exhibit varying degrees of activity for the hydrogenation of phenylacetylene to styrene and ethylbenzene at 51 bar H₂ and 40–100 °C across a variety of solvents. The most active catalysts contain Ga with, formally, a half-filled p_z orbital, and minimal bonding between neighboring Tr₂ or TrTt layers. A 13-layer trigonal polytype of CaGaGe (13T-CaGaGe) was the most active, cyclable, and robust catalyst and under



modest conditions (1 atm H_2 , 40 °C) had a surface specific activity (590 h⁻¹) comparable to a commercial Lindlar's catalyst. Additionally, 13T-CaGaGe maintained 100% conversion of phenylacetylene to styrene at 51 bar H_2 , even after 5 months of air exposure. This work reveals the structural design elements that lead to particularly high catalytic activity in Zintl–Klemm phases, further establishing them as a promising materials platform for hydrogen-based heterogeneous catalysis.

KEYWORDS: intermetallics, catalysis, alkyne hydrogenation, Zintl phase, gallium/main-group

1. INTRODUCTION

The design of new, inexpensive heterogeneous catalysts using earth-abundant elements that can perform complementary chemical transformations to existing systems is essential for long-term sustainability. 1-3 The need to limit the use of precious metals has initiated the discovery of new catalyst concepts and heterogeneous catalyst materials to maximize activity, stability, and selectivity, for which intermetallics have attracted considerable attention.4-7 For example, structurally precise intermetallic alloys such as GaPd2 where precious metals are spatially separated to enhance selectivity, in accordance with the "active-site" isolation concept,8 were found to catalyze the semihydrogenation of acetylene to ethylene with high activities and selectivities. ^{6,9–12} As a second example, many electrides, or compounds that contain excess electrons that preferentially occupy distinct crystallographic sites, have a low work function that can readily reduce substrates such as H₂, and compounds such as LaCoSi have shown promise in NH₃ synthesis.¹³

Most of these intermetallic phases feature transition metals, due to the ease at which they can cycle between coordination environments and oxidation states facilitating the coordinative addition of substrates and elimination of products. Still, there are a large number of intermetallic phases that combine maingroup metals/metalloids with electropositive group 1–3 or lanthanide elements, that form structurally defined covalent

networks in accordance with the Zintl-Klemm concept. These Zintl-Klemm phases have received virtually no attention as catalysts. We recently discovered that BaGa2 showed incredibly high catalytic activities for the semihydrogenation of phenylacetylene to styrene and complete hydrogenation to ethylbenzene, despite the absence of transition metals. 14 We hypothesized that the origin of the catalytic activity stems from the electronic structure of BaGa2, which causes a low barrier for the adsorption of alkynes and dissociative adsorption of H₂.¹⁴ BaGa₂ crystallizes into the AlB₂ structure type. 15 It consists of single-atom-thick honeycomb layers of Ga, with each layer separated by Ba atoms. This compound has a total valence electron count of eight electrons per BaGa2 formula unit, excluding the filled d10 shell. Every Ga has three covalent bonds with its neighbors and can be thought of as being formally reduced to Ga⁻ by Ba²⁺. Thus, the Ga⁻ network is isoelectronic to graphite; each Ga ion is sp2-hybridized and forms a single π -bond with its neighbors. As π -bonding in elements that are in the third row or greater tends to be

Special Issue: Emerging Materials for Catalysis and Energy Applications

Received: June 3, 2021 Accepted: August 11, 2021 Published: August 24, 2021





considerably weaker than σ -bonding, BaGa₂ readily absorbs H₂ at 51 bar H2 and 170 °C to form BaGa2H2, in which every Ga atom is terminated with a Ga-H bond. 15 BaGa2 was found to be a highly active alkyne hydrogenation catalyst, whereas BaGa₂H₂ was not.¹⁴ This suggests that the presence of halffilled p, orbitals in layered honeycomb networks is an important motif necessary for catalytic activity and is necessary for adsorption of the alkyne substrate on the surface. Remarkably, BaGa2 showed surface specific activities that were within an order of magnitude of commercial Pd catalysts and other transition-metal compounds. 14 Analysis of the supernatant immediately after the reaction showed <1 ppm Ga, highlighting the heterogeneous nature of the BaGa2 catalyst.¹⁴ Unfortunately, upon exposure to H₂O or air, BaGa₂ instantaneously formed a surface oxide that inhibited its activity, thereby limiting its long-term use as a catalyst. 14

Once a new catalyst system is discovered, the systematic exploration of the catalytic behavior of numerous closely related analogues is essential for determining the balance between structural and electronic influences on the mechanism, selectivity, and activity to optimize catalytic performance. 16 BaGa2 is just one member in a larger family of Zintl-Klemm phase compounds containing honeycomb networks of main-group elements separated by electropositive cations. 15,17-22 Based on the activity of BaGa2, we thought it relevant to explore whether other members of this family in which at least one of the main-group elements formally has a half-filled p_z orbital (seven valence electrons ignoring any π bonding) could also display similar catalytic activity and would either be more resistant to oxidation or have a more readily removable oxide. We hypothesized that this electronic motif would lead to surfaces with greater Lewis acidity, thereby enhancing the adsorption and subsequent hydrogenation of alkynes. In addition, we sought to probe whether the ability of a phase to absorb H2 into its lattice and form a topotactic hydride as well as the structural and electronic features of the compound would influence catalytic activity and oxide formation. Such features include the planarity of network, the interlayer stacking sequence, whether one or both elements on the honeycomb network formally have seven valence electrons, and if the electropositive cation is divalent or trivalent.

Herein, we compare the catalytic activity of a series of Zintl phases built from honeycomb layers of group 13 triel (Tr) or group 14 tetrel (Tt) networks and having a stoichiometry of ATr_2 and ATrTt (A = Ca, Ba, Y, La, Eu; Tr = Ga, In; Tt = Si, Ge). These compounds have either eight or nine total valence electrons per ATr₂ or ATrTt formula unit. At least one of the triel elements in the network feature a half-filled pz orbital, which again, we consider to be an important electronic feature for alkyne hydrogenation. Most compounds have appreciable catalytic activity in the semihydrogenation of phenylacetylene to styrene at high pressure (51 bar H₂). The most active catalysts contained Ga and lacked any interlayer bonding in the main-group framework, and there was no correlation between the ability to form a known hydride and catalytic activity. For many of these phases, the activity gets disrupted upon exposure to air, due to surface oxidation. However, 13T-CaGaGe, YGa2, and CaGaSi maintained activity after exposure to air. 13T-CaGaGe was the most active, cyclable, and robust catalyst and maintained 100% conversion of phenylacetylene to styrene at 51 bar H₂ even after 5 months of air exposure. Without air exposure, this phase had surface specific activities (SSA) of 590

h⁻¹ at 1 atm H₂ and was selective for the hydrogenation of phenylacetylene to styrene, producing no detectable ethylbenzene within 24 h. Taken together, this work shows that this broad family of layered Zintl phases having triel elements with half-filled p_x orbitals is catalytically active, outlining a new unexplored design feature for transition-metal-free heterogeneous catalysts.

2. EXPERIMENTAL SECTION

2.1. Preparation of Zintl Phase Catalysts. The synthesis of all compounds was performed using air-free conditions whenever possible, and all compounds and elements were prepared and stored in an Ar-filled glovebox. For the synthesis of LaGa2, oil from the lanthanum metal powder (99.9%, Strem) was removed by washing with hexanes several times and allowing it to dry. A total of 1.2 equiv of lanthanum to 2 equiv of gallium (99.99% Strem) was placed in an alumina crucible and sealed in an evacuated quartz tube. The tube was heated to 1100 °C over 10 h and held at that temp for 18 h with the furnace turned off at the end of the synthesis. For the synthesis of orthorhombic EuGa₂ (o-EuGa₂), the oil and oxide on the outside of the europium surface were removed mechanically, and 1.1 equiv of europium (99.9%, Strem) to 2 equiv of gallium was placed in crimped titanium foil and sealed in a quartz tube. The tube was heated in a vertical furnace over 8 h to 900 $^{\circ}\text{C}\text{,}$ held for 20 h, and then cooled over 12 h. For the synthesis of hexagonal EuGa₂ (h-EuGa₂), stoichiometric amounts of europium and gallium were heated in an alumina crucible in a sealed quartz tube to 1050 °C over 6 h, held for about 16 h, and was rapidly quenched. For the synthesis of BaInGe, stoichiometric amounts of indium, germanium, and a 5% excess of barium (99.7% Strem) were added to an alumina crucible and sealed in a quartz tube. The tube was heated up to 900 °C over 6 h, ramped down to 850 °C over 18 h with the furnace shut off after that time.

To synthesize 13T-CaGaGe, CaIn2, and CaGaSi, the surface oxide of the calcium turnings was mechanically removed. Stoichiometric amounts of Ca (99%, Sigma-Aldrich), Ga, Si (99.9999% Strem), In (99.9% Strem), and Ge were placed in a copper hearth and were arcmelted together. The resultant button was flipped so that the materials were melted a total of five times each. A similar process was followed for YGa2, where stoichiometric amounts of yttrium (99.9% Strem) and gallium were arc-melted, flipping between each melt so that button was melted a total of 5 times. To synthesize 4H-CaGaGe, previously synthesized 13T-CaGaGe powder was sealed in an evacuated quartz tube and annealed at 500 °C for 18 h.

2.2. General Procedure for Catalytic Hydrogenations. In 1 bar pressure reactions, the catalytic material is ground in a mortar and pestle and weighed out in an Ar-filled glovebox and then added to a 10 mL round-bottom flask. Anhydrous solvents were then added to the flask. In a typical reaction, ~15 mg of catalyst was added to the flask with 2.5 mL of anhydrous solvent, followed by 0.9 mmol of phenylacetylene substrate. The sealed round-bottom flasks were then removed from the glovebox and placed on hot plates where a H2-filled balloon was added. The H₂ pressure was assumed to be 1 bar. Elevated pressure reactions were done in a similar manner. In a typical reaction, 1.8 mmol of substrate was added to a 20 mL vial along with 20-35 mg of catalyst and 2.5 mL of solvent. These vials were placed in Parr reactors, and once out of the glovebox, hydrogen was added to the desired pressure (51 bar), and the reactors were placed on the heating elements.

Surface specific activities (SSAs) for balloon pressure reactions were calculated using eqs 1-3.

$$SSA = n_0 C / t n_{cat}$$
 (1)

$$n_{\rm cat} = m_{\rm cat} N_{\rm Ga \, sites} / N_{\rm A} \tag{2}$$

$$N_{\text{Ga sites}} = S_{\text{BET}} \times \frac{1 \text{ Ga atom}}{S_{\text{A}}}$$
 (3)

where C is the conversion of the substrate at time t, n_0 is the initial moles of substrate, n_{cat} is the maximum moles of Ga atoms exposed on the surface, $m_{\rm cat}$ is the mass of the catalyst, $N_{\rm Ga~sites}$ is the amount of exposed gallium sites per gram of catalyst, $N_{\rm A}$ is Avogadro's constant, $S_{\rm BET}$ is the specific surface area of the material, and $S_{\rm A}$ is the surface area of the gallium atoms. CaGaGe has 1 Ga atom per 15.3 Ų of surface area for the 001 face of the unit cell; thus, $S_{\rm A}$ would correspond to 15.3 Ų in eq 3.

When comparing catalytic activities between different solvents, all catalysts were used from the same synthetic batches to eliminate differences in the relative amount of oxides, impurities, and surface areas per gram, from synthesis to synthesis.

2.3. Synthesis and Characterization of (Ethynyl-d)benzene. Deuterated phenylacetylene was prepared by loading 1.98 mL (18.0 mmol) and 30.0 mL of dry, distilled hexanes in a 100 mL round-bottom flask in an Ar-filled glovebox. The flask was cooled to $-78\,^{\circ}$ C before the dropwise addition of 13.5 mL of n-butyllithium solution (1.43M, 19.4 mmol) and stirred at this temperature for 30 min. The solution was brought to room temperature, and D_2O (10.0 mL, 554 mmol) was added dropwise over 10 min. The reaction was stirred overnight for 12 h. The reaction mixture was washed with deionized water (3 \times 20 mL) and dried over sodium sulfate. The solvent was removed by rotary evaporation, and deuterium incorporation was determined to be 92% atom %D by 1 H NMR (CDCl₃, 400 MHz, ppm): 3.07 (s, 0.08 H), 7.33 (m, 3H), 7.42 (m, 2H).

2.4. Characterization. Powder X-ray diffraction patterns were obtained at room temperature using a Bruker D8 X-ray powder diffractometer (sealed Cu X-ray tube 40 kV and 40 mA) in Johansson mode.

High performance liquid chromatography was performed with a Shimadzu liquid chromatograph equipped with a reversed phase C18 column and water and acetonitrile as solvents. Ratiometric calibration curves were made to identify ratios of phenylacetylene to styrene to ethylbenzene.

X-ray photoelectron spectra of the samples were taken with a Kratos Ultra X-ray photoelectron spectrometer with a monochromated Al X-ray source. Non-air-exposed powders were prepared in an Ar-filled glovebox, affixed to a sample holder using carbon tape, and loaded into an air-free transfer tool. Energy calibration was performed using the C 1s peak as 284.8 eV.

¹H nuclear magnetic resonance spectroscopy was obtained using a Bruked Avance III 400 MHz spectrometer. CDCl₃ was used as a solvent.

3. RESULTS AND DISCUSSION

A series of Zintl phases were synthesized for the purpose of evaluating their comparative catalytic activities. The crystal structures of these phases are available in Figure 1. We chose to synthesize LaGa₂, YGa₂, BaInGe, o-EuGa₂, h-EuGa₂, CaIn₂, CaGaSi, 4H-CaGaGe, and 13T-CaGaGe to explore the effects of local structure, the presence of interlayer bonding, the potential to form topotactic hydride phases, valence electron count, and electronic structure on catalytic behavior and the propensity for oxidation compared to BaGa₂. Of all these compounds, only LaGa₂, BaGa₂, and BaInGe have been previously reported to react at 150–300 °C, <80 bar H₂ or D₂ to form LaGa₂D_{0.7}, BaGa₂H₂, and BaInGeD, respectively. ^{15,23,24} In previous literature, either decomposition or no formation of hydride phases was observed under similar conditions with CaIn₂, ¹⁵ o-EuGa₂, ^{18,23} CaGaSi, ²⁵ and 4H-CaGaGe ²⁵

The powder diffraction patterns of all compounds are shown in Figures S1–S10. YGa₂, BaInGe, and CaGaSi are all single-phase with no detectable impurity. LaGa₂ has a minor impurity of La₂O₃, which is attributed to its rapid propensity for oxidation (Figure S4). YGa₂ has a trace impurity of Y₂O₃, which inherently exists on the surface of the source Y precursor and proved very challenging to remove (Figure S6). CaIn₂ has a minor impurity of In (Figure S5). BaGa₂ has a minor

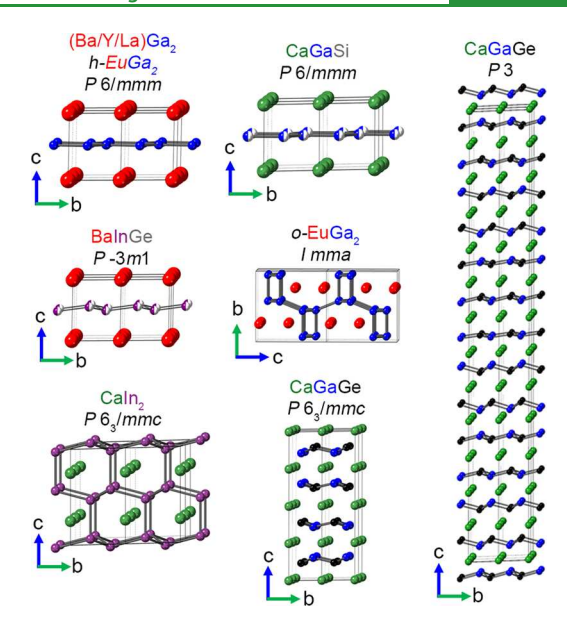


Figure 1. Crystal structures of phases used as catalysts. In all compounds, the main-group network forms a layered honeycomb network of atoms, in which the layers are oriented horizontally and into the page. Ba/Y/La/Eu are depicted as red spheres, Ca is depicted as green spheres, Ga is depicted as blue spheres, In is depicted as purple spheres, Ge is depicted as either black or gray spheres, and Si is depicted as gray spheres. In BaInGe and CaGaSi, the In/Ge and Ga/Si atoms are positioned randomly on the framework.

impurity of BaGa₄, which we previously showed to be catalytic inactive for alkyne hydrogenation. 14 13T-CaGaGe can only be accessed via arc-melting and has ~15% 4H-CaGaGe as a minor impurity phase. The discovery and elucidation of the structure of 13T-CaGaGe is reported in a simultaneously submitted manuscript.²⁶ Both o-EuGa₂ and h-EuGa₂ proved incredibly difficult to grow as pure phases. The h-EuGa2 polymorph could only be formed via fast quenching from 1050 °C, whereas the o-EuGa2 polymorph forms upon slow cooling in agreement with previous reports.²⁷ However, both h-EuGa₂ and o-EuGa₂ always exhibited minor impurities of Eu₃Ga₈ (10 and 8%, respectively) (Figures S3, S8, S11, and S12). Interestingly, the crystal structure of Eu₃Ga₈ can be thought of as a layered intergrowth structure, in which layers of EuGa₄ with tetrahedral Ga are connected to planar honeycomb layers of Ga in h-EuGa₂ (Figure S13).²⁸ It has been established that Eu is divalent in all these compounds.²⁹ In other words, 2/3 of the Ga atoms in the Eu₃Ga₈ are sp²-hybridized with formally seven valence electrons and have the same local planar honeycomb coordination environment as h-EuGa2, which, again, we hypothesize is a structural and electronic feature indicative of catalytic activity.²⁸

By changing the electropositive element in BaGa₂ from barium to europium, we are able to explore how phases that have the same electron count but different bonding arrangements behave catalytically. In particular, the fact that h-EuGa₂ is isostructural to BaGa₂ whereas o-EuGa₂ is not gives us excellent insight into how the different bonding networks behave catalytically. The o-EuGa₂ phase features divalent Eu²⁺ and is distorted into an orthorhombic lattice, in which the intralayer Ga—Ga distance ranges from 2.65 to 2.70 Å, while the interlayer Ga—Ga distances are 2.81 Å. ²⁸ Compared to the intralayer and interlayer distances of BaGa₂ (2.55 and 5.072 Å, respectively) and h-EuGa₂ (2.51 and 4.51 Å, respectively), it is

clear that o-EuGa2 exhibits appreciable interlayer Ga-Ga bonding. CaIn₂ is another phase with significant interlayer bonding. This hexagonal phase has significant puckering in the honeycomb In framework. The intralayer In-In distances are 2.92 Å, while the interlayer distances are 3.13 Å, which is also in the range expected for a covalent In-In bond. 19 Beyond the more subtle structural differences, the group 13 element is changed from gallium to indium to probe its influence on catalysis.

The remaining compounds synthesized all allow us to explore the influence of having one additional valence electron on the honeycomb framework, which would result in only one of the two main-group elements to have a half-filled p_z orbital, rather than both. LaGa2 and YGa2 are isostructural to BaGa2 and have planar honeycomb Ga layers. Replacing divalent Ba2+ with trivalent Y3+ and La3+ gives one more electron per honeycomb layer according to Zintl-Klemm counting rules and nine total valence electrons per formula unit. The ATrTt phases in which A is a divalent cation also feature nine electrons per formula unit. CaGaSi has a planar honeycomb network but with a random configuration of gallium and silicon atoms on the framework. In BaInGe, the In and Ge atoms also randomly occupy both sites of the honeycomb layers, which are slightly distorted away from planarity with In/Ge-In/Ge-In/Ge bond angles of 117.8°. Finally, in CaGaGe, the Ga and Ge atoms occupy distinct positions on the framework and also distort away from planarity. CaGaGe forms two different polytypes, 4H-CaGaGe and 13T-CaGaGe, that are closely related.²⁶ 4H-CaGaGe features puckered honeycomb layers with the Ga and Ge atoms occupying distinct sites. The Ga atoms in neighboring layers are directly on top of each other and are tilted toward each other. Still, the interlayer Ga-Ga distance is 3.577 Å, indicating minimal bonding interactions of the half-filled p_z orbitals. The 13T-CaGaGe structure can be thought of as three unit cells of 4H-CaGaGe, with a 13th misaligned layer, and has interlayer Ga-Ga distances that range from 3.22 to 3.62 Å (with the exception of the misfit layer, which is 4.43 Å). These are much larger than the 2.81 Å interlayer Ga-Ga distances in o-EuGa2, for which interlayer bonding occurs. Thus, 13T-CaGaGe similarly has minimal interlayer bonding interactions between Ga atoms. In addition, the Ga-Ge-Ga bond angles within each honeycomb layer are slightly distorted away from planarity and range from 111.8 to 117.6° in the 13T phase and are 115.2° in the 4H phase. ²⁶ The intra- and interlayer distances, electron count, bond distances, and coordination environment are available in Table S1.

We screened the catalytic activity of the different synthesized phases for the semihydrogenation and hydrogenation of phenylacetylene to styrene and ethylbenzene at 51 bar H₂, with 20-35 mg of catalyst (3.6-8.5 mol %), and under different solvents (n-butanol (n-BuOH), dimethylformamide (DMF), N-methyl pyrrolidone (NMP)) without exposing these catalysts to air (Figure 2). Complete results for these transformations are available in Table S2. Most compounds showed some degree of alkyne semihydrogenation compared to control experiments with no catalyst, which showed less than 5% conversion. An additional control, six-layer rhombohedral CaGe2, showed no activity, signifying the importance of the group 13 Ga or In element in the overall catalysis. 30,31 This allowed us to elucidate general trends that correlate structure and activity. First, the Zintl phases with interlayer bonding between the main-group elements had the least catalytic activity. CaIn2 and o-EuGa2 have interlayer In-

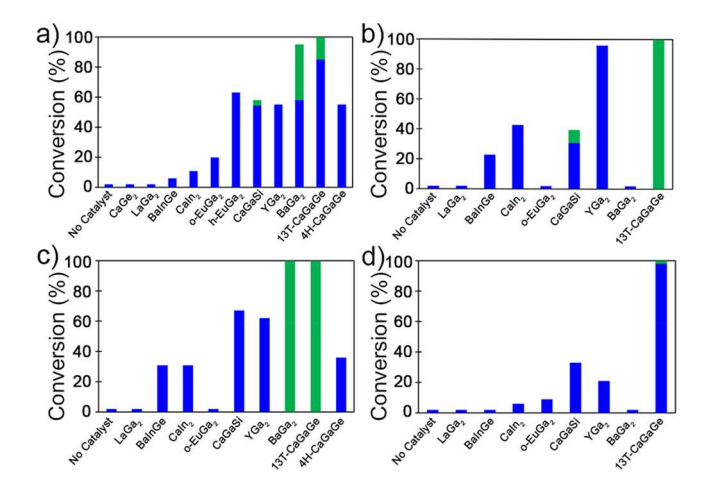


Figure 2. Catalytic activity of different Zintl phases (3.5–8.6 mol %) in the semihydrogenation and hydrogenation of phenylacetylene to styrene and ethylbenzene using 51 bar H₂ in (a) n-BuOH, (b) NMP, (c) DMF, and (d) after 24 h of air exposure in either n-BuOH or DMF(*). Blue represents percent conversion to styrene, and green represents percent conversion to ethylbenzene.

In and Ga—Ga distances within the range expected for covalent bonds but showed the least activity across all three solvents. Considering h-EuGa2 is much more catalytically active than o-EuGa₂ yet contains the same elements, the differences in catalytic activity can be explained by their differences in electronic structure. In particular, the presence of half-filled p_z orbitals in the honeycomb network, as occurs in h-EuGa2, is an essential electronic motif for activity. Furthermore, it is unclear if the trace activity in o-EuGa2 is caused by the Eu3Ga8 impurity, which is present in both compounds, as its crystal structure also contains the same planar honeycomb Ga networks with half-filled 3p₂ orbitals as occurs in h-EuGa₂. The only Zintl-Klemm phase with less activity than CaIn2 and o-EuGa2 without interlayer bonding was LaGa2. The lack of activity of LaGa2 can be explained by its extreme air sensitivity, as it is the only phase that rapidly oxidizes upon immediate exposure to air (Figure S14).

The remaining compounds studied had appreciable activity in the high pressure hydrogenation in n-BuOH, DMF, and NMP. BaInGe showed some activity for the hydrogenation of phenylacetylene, but it was lower than all the gallium compounds. It might be the general case that In-containing phases have reduced activity compared to Ga-containing phases. However, BaInGe is the only known layered honeycomb phase containing indium with a similar electronic structure (i.e., formally having a half-filled In 4pz orbital). Still, BaGa₂, CaGaSi, YGa₂, and 13T/4H-CaGaGe all outperform BaInGe, which helps support the idea that indium is less active.

The four most active catalysts were CaGaSi, YGa2, BaGa2, and 13T-CaGaGe. These compounds have different total valence electrons per formula unit and are either planar or distorted. BaGa2 features eight total valence electrons per formula unit, whereas the other phases have nine total valence electrons per formula unit, thereby indicating that high catalytic activity can be achieved when either one or both of the main-group elements on the framework feature a half-filled p_z orbital. Additionally, 13T-CaGaGe has a puckered honeycomb arrangement of Ga-Ge atoms, whereas CaGaSi, BaGa₂, and YGa2 are all planar, suggesting that catalytic activity does not depend on whether there are small distortions away from

planarity. This is consistent with previous reports that indicate that the electronic structure of the active site and not the geometric structure primarily influences catalytic activity. We have also observed that the most catalytically active phases have the least selectivity, notably in DMF and NMP, which is consistent in the literature. Finally, there is no direct correlation between the high catalytic activity observed in these four compounds and whether the Zintl–Klemm phase can react with H_2 at moderate temperatures and pressures to form a topotactic hydride, as CaGaSi is reported to be unable to form CaGaSiH, whereas BaGa₂ can form BaGa₂H₂. Is,25

Next, we probed how the catalytic properties of these compounds changed upon exposure to air. While as a general rule, Zintl-Klemm phases tend to be air-sensitive and prone to surface oxidation due to the reduced nature of the main-group element, the thermodynamic propensity and rate of oxidation of the surface and in the bulk can significantly vary between compounds. The presence of oxide phases was not detected in the XRD patterns for almost all phases after exposure to air, with the exception of LaGa₂, which starts to form La(OH)₃ and Ga₂O₃ impurities after 2 h of exposure to air (Figure S14). We attribute the trace Y₂O₃ impurity in YGa₂ to be a result of the surface oxide on the Y source, as the intensity of the Y₂O₃ reflections in the XRD pattern does not increase after air exposure (Figure S15). Still, most compounds had a drop off in catalytic activity upon exposure to air for 1 day, implying the formation of a surface oxide layer that disrupts catalysis. XPS was used to compare the changes to the surface of the most active gallium compounds, 13T-CaGaGe, YGa2, and BaGa2, before and after their exposure to air (Figure 3), focusing on the Ga 2p_{3/2} peak. Before air exposure, when all compounds are highly active, all three compounds have a 2p_{3/2} low energy shoulder centered at 1115.4-1115.7 eV that is indicative of an anionic Ga species, as would be expected in these layered Zintl-Klemm phases. All compounds also exhibit dominant 2p_{3/2} peaks centered at ~1117.1-1117.9 eV, and 13T-CaGaGe and YGa2 featured a more oxidized peak centered at 1119.8-1120.2. Both of these peaks correspond to the varying degrees of Gan+ surface oxidation that may occur with the native oxide.^{33–35} The presence of the low energy shoulder was previously found to be an essential indicator for catalytic activity in BaGa₂. ¹⁴ The relative area of this low energy shoulder before air exposure is 16, 34, and 11% for BaGa₂, 13T-CaGaGe, and YGa2, respectively. Upon exposure to air for 2 h, the low energy shoulder disappears in BaGa2; however, it still remains prevalent in both 13T-CaGaGe and YGa2 at 24 and 12%, respectively. YGa2 and 13T-CaGaGe both show catalytic activity upon air exposure, while BaGa2 does not, further showing that the low energy shoulder correlates with catalytic activity in these other phases and that the different Zintl phases can have differing rates of surface oxidation.

13T-CaGaGe is by far the most active Zintl–Klemm catalyst, demonstrating complete semihydrogenation from phenylacetylene to styrene in *n*-BuOH and complete hydrogenation to ethylbenzene in NMP and DMF in our initial 51 bar H₂ tests. What is most remarkable about this phase is its enhanced air stability and long-term recyclability. We probed the recyclability of the same 13T-CaGaGe catalyst in phenylacetylene semihydrogenation after seven 24 h cycles at 51 bar H₂ in *n*-BuOH. When switching reagents, the same catalyst was exposed to air between each cycle for durations of 2–24 h (Figure 4). Compared to BaGa₂, which would lose all catalytic activity upon instantaneous air exposure, 13T-

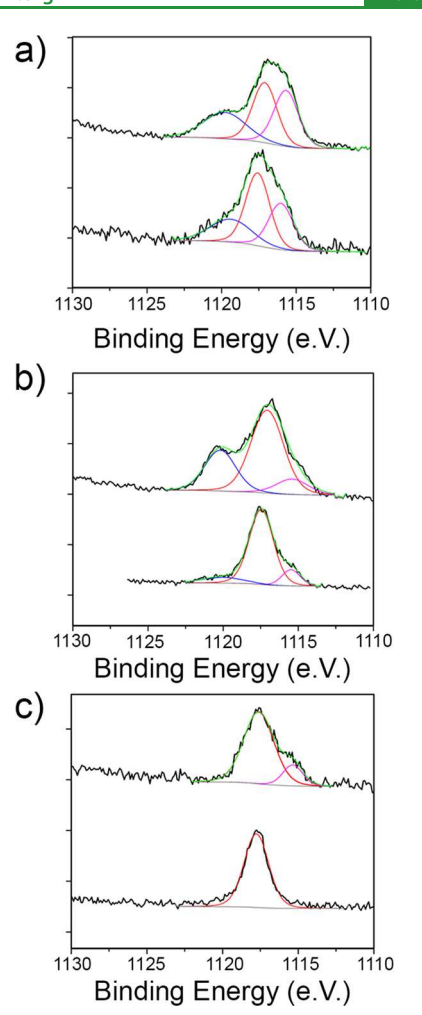


Figure 3. X-ray photoelectron spectra of the Ga $2p_{3/2}$ peak of (a) 13T-CaGaGe, (b) YGa₂, and (c) BaGa₂ before (top) and after (bottom) air exposure. The fitting of the reduced Ga⁻ was at ~1115.5 eV, and the more oxidized Ga peaks were at ~1117.1–1117.9 and 1119.8–1120.2 eV.

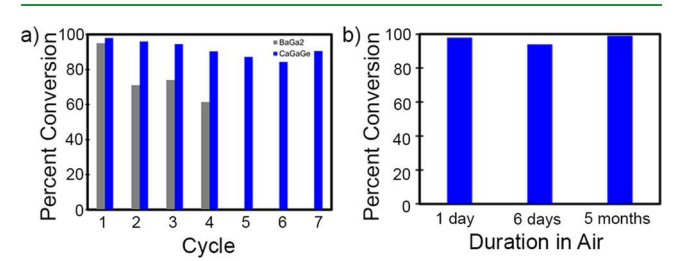


Figure 4. (a) Catalyst recyclability study for 13T-CaGaGe (blue) compared to $BaGa_2$ (gray) showing greater that 90% conversion of phenylacetylene to styrene and after seven cycles for the same CaGaGe catalyst at 51 bar H_2 , n-BuOH, 90 °C, 20 h, and 8.1 mol % (starting). (b) Catalyst air stability study for CaGaGe after 1 day, 6 days, and 5 months of air exposure to the CaGaGe powder (51 bar H_2 , n-BuOH, 90 °C, 20 h, 6.5–8.1 mol %).

CaGaGe maintains a much higher conversion with more cycles, and even has 90% conversion after seven cycles. To further probe the air stability of this catalyst, we explored whether any changes in percent conversion occurred after exposing to air after 1 day, 6 days, and 5 months, using the same 51 bar reaction conditions. Remarkably, ~100% conversion to styrene is observed even after 5 months of

exposure to air. This resilience of the catalytic activity to prolonged air exposure is unprecedented among these Zintl–Klemm phases. Finally, we explored the *cis-/trans*-selectivity of this 13T-CaGaGe using phenylacetylene, in which the terminal acetylenic hydrogen was deuterated (Figure S16). After a \sim 20 h, 51 bar H₂ hydrogenation reaction, ^1H NMR analysis of the styrene product indicated a 88:12% *cis:trans*-selectivity.

13T-CaGaGe also catalyzes the semihydrogenation of phenylacetylene to styrene under much milder conditions (1 bar $\rm H_2$, 40 °C, 8.5 mol % 13T-CaGaGe, 23 h), again with no detectable ethylbenzene formation. Catalytic activity was observed in a variety of solvents at 1 bar $\rm H_2$ (Table 1), with

Table 1. Conversion of Phenylacetylene Hydrogenation to Styrene in the Listed Anhydrous Solvents^a

solvent	conversion (%)
NMP	100
<i>n</i> -butanol	60
DMF	52
1,4-dioxane	14
IPA	18
ethanol	23

 $^{\prime }40$ °C, 23 h, 8.5 mol % ($\sim \! 15$ mg) 13T-CaGaGe catalyst, 0.91 mmol of phenylacetylene.

complete conversion occurring in anhydrous NMP, with non-air-exposed catalyst. The next best solvents are *n*-BuOH and DMF, for which >50% conversion of phenylacetylene to styrene was achieved after 23 h. As shown in the conversion vs time (Figure 5), complete conversion of phenylacetylene to

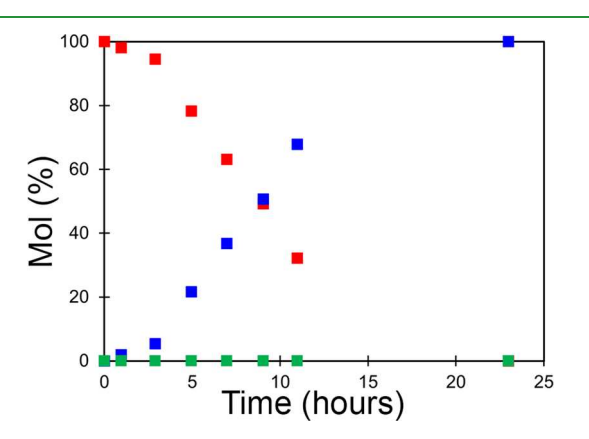


Figure 5. Time-dependent conversion of phenylacetylene to styrene in NMP at 1 bar $\rm H_2$, 40 °C, 0.91 mmol of phenylacetylene, 2.5 mL of NMP, and 15 mg of 13T-CaGaGe. Red squares represent phenylacetylene, blue squares represent styrene, and green squares represent ethylbenzene. The SSA was calculated from the 5 h time point, which includes the induction period and thus represents a lower bound.

styrene occurred well within 23 h in NMP. While this reaction was selective to styrene within the first day, ethylbenzene was observed after 48 h. This suggests that ethylbenzene formuation occurs via a two-step process. The surface specific activity (SSA) in NMP was determined by measuring the surface area per gram of catalyst using the Kr adsorption isotherm analyzed via the Braunauer–Emmett–Teller (BET) method (Figure S17), along with the conversion vs time. The surface area of 13T-CaGaGe was determined to be 0.406 m² g⁻¹. Assuming that Ga is the only catalytically active site, the

SSA is estimated to be 590 h⁻¹, using the 5 h time point in Figure 5. It is important to point out that in both solvents, the time-dependent conversion indicates the presence of an induction period, which makes the estimate of SSA a lower bound and significantly complicates further kinetic analysis and determination of the order of the reaction with respect to phenylacetylene. An induction period was also similarly observed in BaGa2, but ICP-OES analysis of the supernatant indicated the amount of soluble Ga to be <1 ppm, suggesting that catalysis is not due to a soluble Ga-based impurity. ¹⁴ The XRDs pre and postcatalysis are also virtually superimposable (Figure S18). The 13T-CaGaGe SSA is higher than what was previously reported for BaGa₂ (425 h⁻¹) and is relatively close to a Lindlar's catalyst control (650 h⁻¹) (Figure \$19). Thus, 13T-CaGaGe dethrones BaGa2 as the most active Pt/Pd-free heterogeneous catalyst for phenylacetylene hydrogenation and has comparable activities with Pd. For comparison, the SSAs of other phenylacetylene hydrogenation catalysts under similar conditions are listed in Table S3.

4. CONCLUSION

This work shows that a broad of family of electronic and structurally similar layered Zintl-Klemm ATr₂ and ATrTt phases can catalyze the hydrogenation and semihydrogenation of phenylacetylene with varying activities. The common feature in the electronic structure of these materials that is necessary for catalytic activity is the presence of a triel element on the honeycomb lattice that would formally have a half-filled p_z orbital, bestowing Lewis acidity onto the framework. The most active catalysts lacked any interlayer bonding. Furthermore, the ability to form bulk metal hydride phases did not correlate with activity. While all compounds lost some degree of catalytic activity upon exposure to air, 13T-CaGaGe remained highly active in high-pressure hydrogenation reactions. Without exposure to air, 13T-CaGaGe had SSAs comparable to Lindlar's catalyst at 1 bar H2 and were among the largest for non-Pd/Pt catalysts. Furthermore, this work establishes precedent to investigate other isoelectronic Zintl phase catalysts, including those that contain Al. This discovery that this family of materials universally catalyzes alkyne hydrogenation paves the way for future surface science studies on the origin of catalytic behavior in these compounds, as well as expansion of the reaction and substrate scope, 36 and optimization of long-term catalytic performance.

ASSOCIATED CONTENT

Supporting Information

The Supporting Information is available free of charge at https://pubs.acs.org/doi/10.1021/acsami.1c10358.

Experimental methods, X-ray diffraction patterns of all phases, BET measurements, crystal structure of Eu₃Ga₈ impurity, and Rietveld refinements of the h-EuGa₂ and o-EuGa₂ (PDF)

AUTHOR INFORMATION

Corresponding Author

Joshua E. Goldberger – Department of Chemistry and Biochemistry, The Ohio State University, Columbus, Ohio 43210, United States; ⊚ orcid.org/0000-0003-4284-604X; Email: goldberger.4@osu.edu

Author

Kelsey L. Hodge - Department of Chemistry and Biochemistry, The Ohio State University, Columbus, Ohio 43210, United States

Complete contact information is available at: https://pubs.acs.org/10.1021/acsami.1c10358

Author Contributions

The manuscript was written through contributions of all authors.

Notes

The authors declare no competing financial interest.

ACKNOWLEDGMENTS

This manuscript is dedicated to the memory of Chia-King Frank Tsung, a creative and inspiring scientist, colleague, and friend. This work was primarily supported by the Center of Emergent Materials, an NSF MRSEC, under award number DMR-2011876. We gratefully acknowledge C. Bien and C. R. Wade for their assistance with BET measurements.

REFERENCES

- (1) Sheldon, R. A. Engineering a More Sustainable World Through Catalysis and Green Chemistry. J. R. Soc., Interface 2016, 13, 20160087.
- (2) Ludwig, J. R.; Schindler, C. S. Catalyst: Sustainable Catalysis. Chem. 2017, 2, 313-316.
- (3) Descorme, C.; Gallezot, P.; Geantet, C.; George, C. Heterogeneous Catalysis: A Key Tool Toward Sustainability. ChemCatChem 2012, 4, 1897-1906.
- (4) Furukawa, S.; Komatsu, T. Intermetallic Compounds: Promising Inorganic Materials for Well-Structured and Electronically Modified Reaction Environments for Efficient Catalysis. ACS Catal. 2017, 7,
- (5) Dasgupta, A.; Rioux, R. M. Intermetallics in Catalysis: An Exciting Subset of Multimetallic Catalysts. Catal. Today 2019, 330,
- (6) Armbrüster, M. Intermetallic Compounds in Catalysis a Versatile Class of Materials Meets Interesting Challenges. Sci. Technol. Adv. Mater. 2020, 21, 303-322.
- (7) Pei, Y.; Zhang, B.; Maligal-Ganesh, R. V.; Naik, P. J.; Goh, T. W.; Macmurdo, H. L.; Qi, Z.; Chen, M.; Behera, R. K.; Slowing, I. I.; Huang, W. Catalytic Properties of Intermetallic Platinum-Tin Nanoparticles with Non-Stoichiometric Compositions. J. Catal. 2019, 374, 136-142.
- (8) Verbeek, H. S.; W, M. H. The Study of the Alloys of Platinum and Tin by Chemisorption. J. Catal. 1976, 42, 257-267.
- (9) Matselko, O.; Zimmermann, R. R.; Ormeci, A.; Burkhardt, U.; Gladyshevskii, R.; Grin, Y.; Armbrüster, M. Revealing Electronic Influences in the Semihydrogenation of Acetylene. J. Phys. Chem. C **2018**, 122, 21891-21896.
- (10) Armbrüster, M.; Kovnir, K.; Behrens, M.; Teschner, D.; Grin, Y.; Schlögl, R. Pd-Ga Intermetallic Compounds as Highly Selective Semihydrogenation Catalysts. J. Am. Chem. Soc. 2010, 132, 14745-
- (11) Grin, Y.; Armbrüster, M.; Baranov, A. I.; Finzel, K.; Kohout, M.; Ormeci, A.; Rosner, H.; Wagner, F. R. Atomic Interactions in the Intermetallic Catalyst GaPd. Mol. Phys. 2016, 114, 1250-1259.
- (12) Kovnir, K.; Osswald, J.; Armbrüster, M.; Giedigkeit, R.; Ressler, T.; Grin, Y.; Schlögl, R. PdGa and Pd₃Ga₇: Highly-Selective Catalysts for the Acetylene Partial Hydrogenation. Stud. Surf. Sci. Catal. 2006, 162, 481-488.
- (13) Gong, Y. T.; Wu, J. Z.; Kitano, M.; Wang, J. J.; Ye, T. N.; Li, J.; Kobayashi, Y.; Kishida, K.; Abe, H.; Niwa, Y.; Yang, H. S.; Tada, T.; Hosono, H. Ternary Intermetallic LaCoSi as a Catalyst for N2 Activation. Nat. Catal. 2018, 1, 178-185.

- (14) Hodge, K. L.; Goldberger, J. E. Transition Metal-Free Alkyne Hydrogenation Catalysis with BaGa2, a Hydrogen Absorbing Layered Zintl Phase. J. Am. Chem. Soc. 2019, 141, 19969-19972.
- (15) Björling, T.; Noréus, D.; Häussermann, U. Polyanionic Hydrides from Polar Intermetallics AeE₂ (Ae = Ca, Sr, Ba; E = Al, Ga, In). J. Am. Chem. Soc. 2006, 128, 817-824.
- (16) Meyer, R. J.; Zhang, Q.; Kryczka, A.; Gomez, C.; Todorovic, R. Perturbation of Reactivity with Geometry: How Far Can We Go? ACS Catal. 2018, 8, 566-570.
- (17) Zapp, N.; Auer, H.; Kohlmann, H. YHO, an Air-Stable Ionic Hydride. Inorg. Chem. 2019, 58, 14635-14641.
- (18) Wenderoth, P.; Kohlmann, H. In Situ Neutron Powder Diffraction of the Formation of SrGa₂D₂, and Hydrogenation Behavior of YbGa₂ and EuGa₂. Inorg. Chem. 2013, 52, 10525-10531.
- (19) Nuspl, G.; Polborn, K.; Evers, J.; Landrum, G. A.; Hoffmann, R. The Four-Connected Net in the CeCu₂ Structure and Its Ternary Derivatives. Its Electronic and Structural Properties. Inorg. Chem. 1996, 35, 6922-6932.
- (20) Evans, M. J.; Wu, Y.; Kranak, V. F.; Newman, N.; Reller, A.; Garcia-Garcia, F. J.; Haussermann, U. Structural Properties and Superconductivity in the Ternary Intermetallic Compounds MAB (M = Ca, Sr, Ba; A = Al, Ga, In; B = Si, Ge, Sn). Phys. Rev. B: Condens. Matter Mater. Phys. 2009, 80, 064514.
- (21) Bojin, M. D.; Hoffmann, R. The REME Phases II. What's Possible? Helv. Chim. Acta 2003, 86, 1683-1708.
- (22) Bojin, M. D.; Hoffmann, R. The REME Phases I. An Overview of Their Structural Variety. Helv. Chim. Acta 2003, 86, 1653-1682.
- (23) Werwein, A.; Benndorf, C.; Bertmer, M.; Franz, A.; Oeckler, O.; Kohlmann, H. Hydrogenation Properties of LnAl₂ (Ln = La, Eu, Yb), LaGa₂, LaSi₂ and the Crystal Structure of LaGa₂H_{0.71(2)}. Crystals 2019,
- (24) Evans, M. J.; Kranak, V. F.; Garcia-Garcia, F. J.; Holland, G. P.; Daemen, L. L.; Proffen, T.; Lee, M. H.; Sankey, O. F.; Häussermann, U. Structural and Dynamic Properties of BaInGeH: A Rare Solid-State Indium Hydride. Inorg. Chem. 2009, 48, 5602-5604.
- (25) Evans, M. J.; Holland, G. P.; Garcia-Garcia, F. J.; Häussermann, U. Polyanionic Gallium Hydrides from AlB2-Type Precursors AeGaE (Ae = Ca, Sr, Ba; E= Si, Ge, Sn). J. Am. Chem. Soc. 2008, 130, 12139-
- (26) Hodge, K. L.; Gray, M. B.; Windl, W.; Goldberger, J. E. Lucky Number 13: A 13-layer Polytype of the Alkyne Hydrogenation Catalyst, CaGaGe. Submitted.
- (27) Buschow, K. H. J.; De Mooij, D. B. Note on the Crystal Structure of EuGa2. J. Less-Common Met. 1984, 97, L5-L8.
- (28) Demooij, D. B.; Buschow, K. H. J. The Crystal-Structure Eu₃Ga₈. J. Less-Common Met. 1985, 109, 117-122.
- (29) De Vries, J. W. C.; Thiel, R. C.; Buschow, K. H. J. Magnetic Properties and 151Eu Mössbauer Effect Studied in Eu-Ga and Eu-Sn Intermetallic Compounds. Physica B+C 1985, 128, 265-272.
- (30) Cultrara, N. D.; Wang, Y. X.; Arguilla, M. Q.; Scudder, M. R.; Jiang, S. S.; Windl, W.; Bobev, S.; Goldberger, J. E. Synthesis of 1T, 2H, and 6R Germanane Polytypes. Chem. Mater. 2018, 30, 1335-
- (31) Bianco, E.; Butler, S.; Jiang, S.; Restrepo, O. D.; Windl, W.; Goldberger, J. E. Stability and Exfoliation of Germanane: A Germanium Graphane Analogue. ACS Nano 2013, 7, 4414-4421.
- (32) Mironenko, R. M.; Belskaya, O. B.; Likholobov, V. A. Approaches to the synthesis of Pd/C catalysts with controllable activity and selectivity in hydrogenation reactions. Catal. Today 2020, 357, 152-165.
- (33) Romo-Garcia, F.; Higuera-Valenzuela, H. J.; Cabrera-German, D.; Berman-Mendoza, D.; Ramos-Carrazco, A.; Contreras, O. E.; Garcia-Gutierrez, R. Gallium Nitride Thin Films by Microwave Plasma-Assisted ALD. Opt. Mater. Express 2019, 9, 4187-4193.
- (34) Lin, Y.-J.; Tsai, C.-D.; Lyu, Y.-T.; Lee, C.-T. X-ray Photoelectron Spectroscopy Study of (NH₄)₂S_x-Treated Mg-Doped GaN Layers. Appl. Phys. Lett. 2000, 77, 687-689.

(35) Cybulskis, V. J.; Pradhan, S. U.; Lovon-Quintana, J. J.; Hock, A. S.; Hu, B.; Zhang, G. H.; Delgass, W. N.; Ribeiro, F. H.; Miller, J. T. The Nature of the Isolated Gallium Active Center for Propane Dehydrogenation on Ga/SiO₂. Catal. Lett. 2017, 147, 1252–1262. (36) Pei, Y.; Chen, M.; Zhong, X.; Zhao, T. Y.; Ferrer, M.-J.; Maligal-Ganesh, R. V.; Ma, T.; Zhang, B.; Qi, Z.; Zhou, L.; Bowers, C. R.; Liu, C.; Huang, W. Pairwise Semi-Hydrogenation of Alkyne to Cis-alkene on Platinum-Tin Intermetallic Compounds. Nanoscale 2020, 12, 8519–8524.